ELEMENTA
Science of the Anthropocene

O_3, CH_4, CO_2, CO, NO_2 and NMHC aircraft measurements in the Uinta Basin oil and gas region under low and high ozone conditions in winter 2012 and 2013

S. J. Oltmans[1,2*] • A. Karion[1,2,6] • R. C. Schnell[2] • G. Pétron[1,2] • D. Helmig[3] • S. A. Montzka[2] • S. Wolter[1,2] • D. Neff[1,2] • B. R. Miller[1,2] • J. Hueber[3] • S. Conley[4,5] • B. J. Johnson[2] • C. Sweeney[1,2]

[1]CIRES, University of Colorado, Boulder, Colorado, United States
[2]NOAA/ESRL, Global Monitoring Division, Boulder, Colorado, United States
[3]Institute of Arctic and Alpine Research (INSTAAR), University of Colorado, Boulder, Colorado, United States
[4]University of California, Davis, California, United States
[5]Scientific Aviation, Boulder, Colorado, United States
[6]National Institute of Standards and Technology, Gaithersburg, Maryland, United States
*samuel.j.oltmans@noaa.gov

Abstract

Instrumented aircraft measuring air composition in the Uinta Basin, Utah, during February 2012 and January-February 2013 documented dramatically different atmospheric ozone (O_3) mole fractions. In 2012 O_3 remained near levels of ~40 ppb in a well-mixed 500–1000 m deep boundary layer while in 2013, O_3 mole fractions >140 ppb were measured in a shallow (~200 m) boundary layer. In contrast to 2012 when mole fractions of emissions from oil and gas production such as methane (CH_4), non-methane hydrocarbons (NMHCs) and combustion products such as carbon dioxide (CO_2) were moderately elevated, in winter 2013 very high mole fractions were observed. Snow cover in 2013 helped produce and maintain strong temperature inversions that capped a shallow cold pool layer. In 2012, O_3 and CH_4 and associated NMHCs mole fractions were not closely related. In 2013, O_3 mole fractions were correlated with CH_4 and a suite of NMHCs identifying the gas field as the primary source of the O_3 precursor NMHC emissions. In 2013 there was a strong positive correlation between CH_4 and CO_2 suggesting combustion from oil and natural gas processing activities. The presence of O_3 precursor NMHCs through the depth of the boundary layer in 2013 led to O_3 production throughout the layer. In 2013, O_3 mole fractions increased over the course of the week-long episodes indicating O_3 photochemical production was larger than dilution and deposition rates, while CH_4 mole fractions began to level off after 3 days indicative of some air being mixed out of the boundary layer. The plume of a coal-fired power plant located east of the main gas field was not an important contributor to O_3 or O_3 precursors in the boundary layer in 2013.

Managing Editor-in-Chief
Michael E. Chang,
Georgia Institute of Technology

Guest Editor
Brian Lamb,
Washington State University

Knowledge Domain
Atmospheric Science

Article Type
Research Article

Part of an *Elementa* Special Forum
Oil and Natural Gas Development: Air Quality, Climate Science, and Policy

Received: March 24, 2016
Accepted: September 13, 2016
Published: October 28, 2016

Introduction

Vigorous ozone formation in the summer under conditions with high levels of solar insolation and abundant O_3 precursor chemicals has long been recognized (Chameides et al., 1992). High levels of O_3 production during winter has only recently been documented in locations such as the Upper Green River Basin, Wyoming and Uinta Basin, Utah, in association with effluents from oil and gas production operations (Schnell et al., 2009; Oltmans et al., 2014; Rappenglück et al., 2014). In these basins, the strong role of meteorology, topography, and high levels of O_3 precursors from oil and gas extraction activities have been identified as key drivers of the wintertime high O_3 events (ibid.). The presence of snow-cover acts as both an enhancer of available ultraviolet (UV) radiation by greatly increasing the surface albedo

and as a promoter of strong temperature inversions that trap O_3 precursor emissions in a shallow cold pool surface-based layer (Bader and McKee, 1985; Yu and Pielke, 1986; Schnell et al., 2009; Lareau et al., 2012; Oltmans et al., 2014).

In 2012 and 2013, a multi-agency Uinta Basin Winter Ozone Study (UBWOS) took place in the Uinta Basin in NE Utah (Figure 1) (Lyman and Shorthill, 2013; Stoeckenius and McNally, 2014). Measurements included hundreds of ozone profiles through the boundary layer from tethered ozonesondes (Schnell et al., 2016), non-methane hydrocarbon (NMHC) and nitrogen oxide mole fraction vertical profiles (Helmig et al., 2014), surface chemical constituent observations, and meteorological measurements (Lyman and Shorthill, 2013; Edwards et al., 2013; Stoeckenius and McNally, 2014; Edwards et al., 2014). In the Uinta Basin, intense natural gas production is located mainly on the east side of the Basin and oil production primarily on the west side. Natural gas production levels were similar in 2012 and 2013 with ~18% greater oil production in 2013 (Utah Oil and Gas Program). Emissions from oil and gas production and processing activities as well as combustion emissions associated with vehicle traffic, drilling rigs, compressor stations and gas processing may be significant sources of both volatile organic compounds (VOCs) (Gilman et al., 2013; Warneke et al., 2014) and nitrogen oxides ($NO_x = NO + NO_2$), primary O_3 precursors.

This paper presents unique sets of aircraft collected data in the winters of 2012 and 2013 in the Uinta Basin under contrasting meteorological conditions. In the winter of 2012 there were no periods of persistent snow-covered ground in the Uinta Basin and no large enhancements in O_3 while in 2013 the ground was snow-covered during January and February (Oltmans et al., 2014).

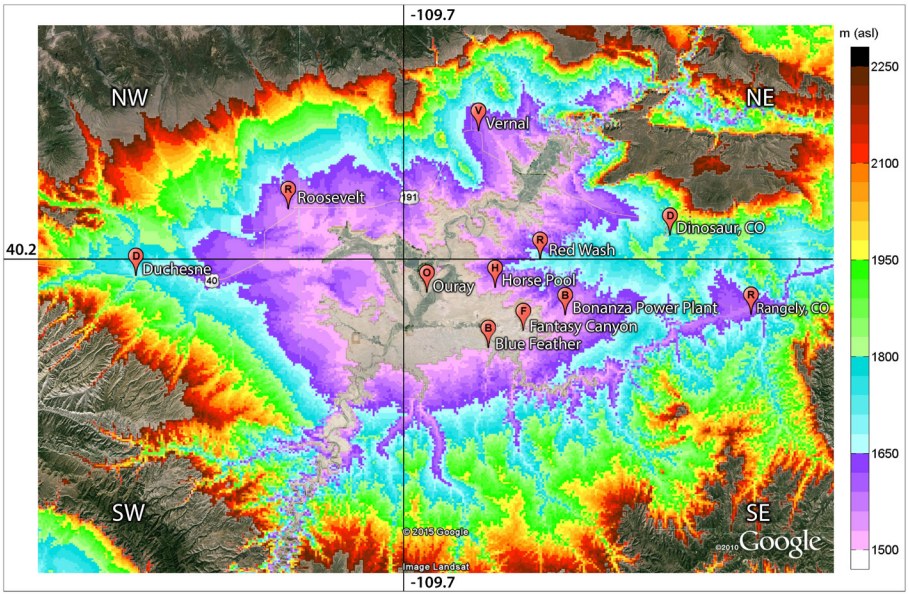

Figure 1

Topography of the Uinta Basin.

The locations of surface measurement sites and several towns in the basin are also shown. The border between the aqua and purple colors is at 1650 m asl.

doi: 10.12952/journal.elementa.000132.f001

Methodologies

In 2012 aircraft measurements were conducted with a single-engine Mooney TLS aircraft (operated by Scientific Aviation; http://www.scientificaviation.com/) and in 2013 a single-engine Cessna 210 aircraft (operated by Kalscott Engineering; http://www.kalscott.com). Instruments drew air through dedicated inlets installed under the aircrafts' starboard wings (Figure S1). On-board instrumentation included high-frequency analyzers for carbon monoxide (CO) (2013 only), carbon dioxide (CO_2), methane (CH_4), and water vapor (H_2O) (Picarro G2401m), nitrogen dioxide (NO_2) (Los Gatos Research Model 911-0009), and ozone (O_3) (2B Technologies Model 211). NOAA GMD glass flask packages were used to collect discrete air samples that were analyzed for a number of trace gases including CO, CO_2, CH_4, C_3H_8 (propane), C_4H_{10} (butane), C_5H_{12} (pentane), C_2H_2 (acetylene), C_6H_6 (benzene) (2012 only) and C_2H_6 (ethane), hexane isomers, and toluene (Helmig et al., 2009, 2014). GPS location, temperature, relative humidity, and ambient pressure collected onboard were synchronized with the gas measurements.

Measurements of trace gases both from the in-situ continuous analyzers and the flask packages are reported on the NOAA/WMO scales as dry air mole fractions (moles per mole of dry air), using methods outlined in Karion et al. (2013a) and online (NOAA GMD Aircraft). O_3 and NO_2 mixing ratios (measured with respect to ambient air) are equivalent to mole fractions when referred to dry air and are denoted herein as mole fractions. In 2012, ozone measurements were made with a 2B Technologies UV photometric analyzer with the solid phase scrubber. In 2013, measurements of O_3 were made with a 2B Technology analyzer that used nitric oxide (NO) in place of a solid phase scrubber to avoid potential

inference from aromatics and mercury (Ollison et al., 2014). The O_3 instruments were calibrated before and after each campaign against a NOAA GMD standard that is regularly compared with a U.S. NIST standard. The Los Gatos Research NO_2 instrument was factory calibrated prior to the field deployment.

In 2012 ten research flights were conducted over the period 3-18 February with daytime surface temperatures at or above freezing, snow free ground, and a well-mixed boundary layer (Lyman and Shorthill, 2013). In 2013 seven research flights were conducted over an 8-day period from 31 January to 7 February. In 2013 snow-covered ground, sub-freezing surface temperatures (dipping to below -10° C) low wind speeds, and limited cloud cover supported stable shallow cold pools (~200 m at their deepest) capped by highly stratified temperature inversions.

Results

Since there was no appreciable photochemical O_3 production in winter 2012, flights focused on determining emissions from oil and gas activities, primarily over the main gas field (Karion et al., 2013b). In 2013, flights were conducted during an episode of intense O_3 production in which the spatial and temporal features of O_3, CH_4, and O_3 precursor NMHCs mole fractions were characterized. During this 8-day period in 2013, surface ozone hourly mole fractions built up from approximately background levels of 45 ppb to over 140 ppb (Figure 2). The first flight of the study (conducted on 31 January) occurred three days after O_3 rich air from a prior event had been flushed out of the Basin by a frontal system. The final flight on 7 February took place during the early stages of an incursion of a Pacific air mass that again flushed O_3 and oil and natural gas field emissions out of the Basin in the subsequent 2 days.

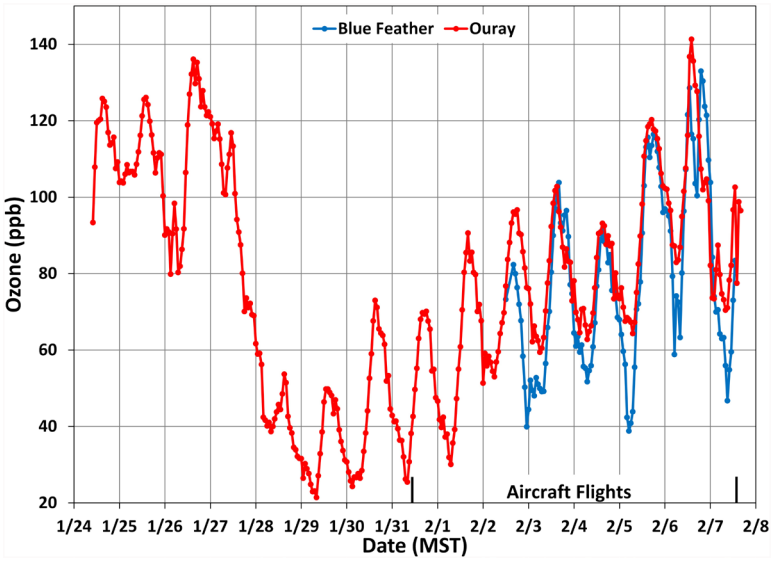

Figure 2

Hourly surface ozone mole fractions in January-February 2013.

Observations from the Blue Feather (blue) and Ouray (red) sites in the Uinta Basin The period of the aircraft flights from 31 Janurary to 8 February is indicated.

doi: 10.12952/journal.elementa.000132.f002

Vertical profiles of O_3, CO_2, CH_4 and CO in relation to temperature profiles

The contrasting vertical temperature structure within the Basin in 2012 and 2013 played a significant role in the way gaseous constituents were distributed both vertically and across the Basin. Typical profiles obtained at a number of locations on 9 February 2012 (Figure 3a) show consistent temperature structure across the Uinta Basin (Figure 3b) with temperature decreasing with altitude. Profiles are plotted with respect to altitude above sea level (asl) to provide consistent altitude registration for the different profiles as terrain varies across the Basin. Also, in 2012 (Figure 3c) O_3 mole fractions fell within a relatively narrow range (~30–40 ppb) in the sampled altitude range. The highest CH_4 and CO_2 mole fractions (Figure 3d and e) were constrained within the layer that was capped at ~2000 m asl.

In contrast on 6 February 2013 (Figure 4), the flight day with the highest O_3 mole fractions observed by the aircraft, O_3 in all four profiles was generally >100 ppb below 1650 m asl. Above ~1800 m asl there was a gradual decrease in all of the constituents with the mole fractions approaching the lower free tropospheric values at ~2200 m asl where the temperature lapse rate became positive (decreasing temperature with altitude) (Figure 4b). This suggests there was a transition zone resulting from the slow mixing of the higher mole fractions of CH_4 and O_3 out of the top of the boundary layer into the free troposphere. A cold pool layer with a top at 1650–1700 m asl containing the highest constituent mole fractions with a layer of decreasing constituent mole fractions above was characteristic of all of the flights in winter 2013 (Figure S2).

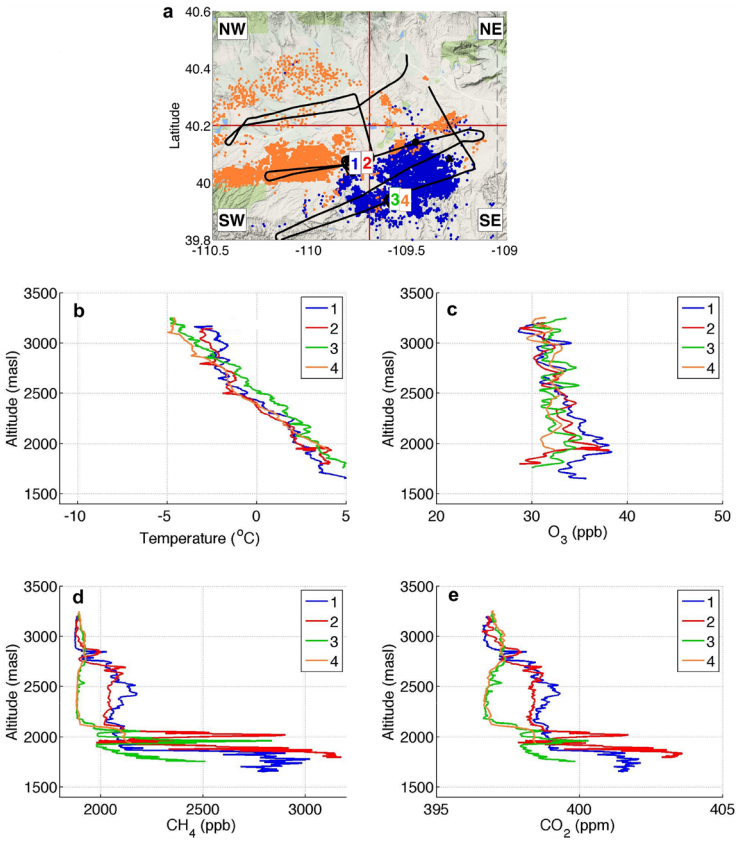

Figure 3

Vertical profile measurements in the Uinta Basin on 9 Feb. 2012.

Panel (a) Map of flight tracks and location of: (b) Temperature profiles, (c) O_3 profiles, (d) CH_4 profiles, (e) CO_2 profiles. Oil well locations are shown on the map as orange dots and gas wells as blue dots.

doi: 10.12952/journal.elementa.000132.f003

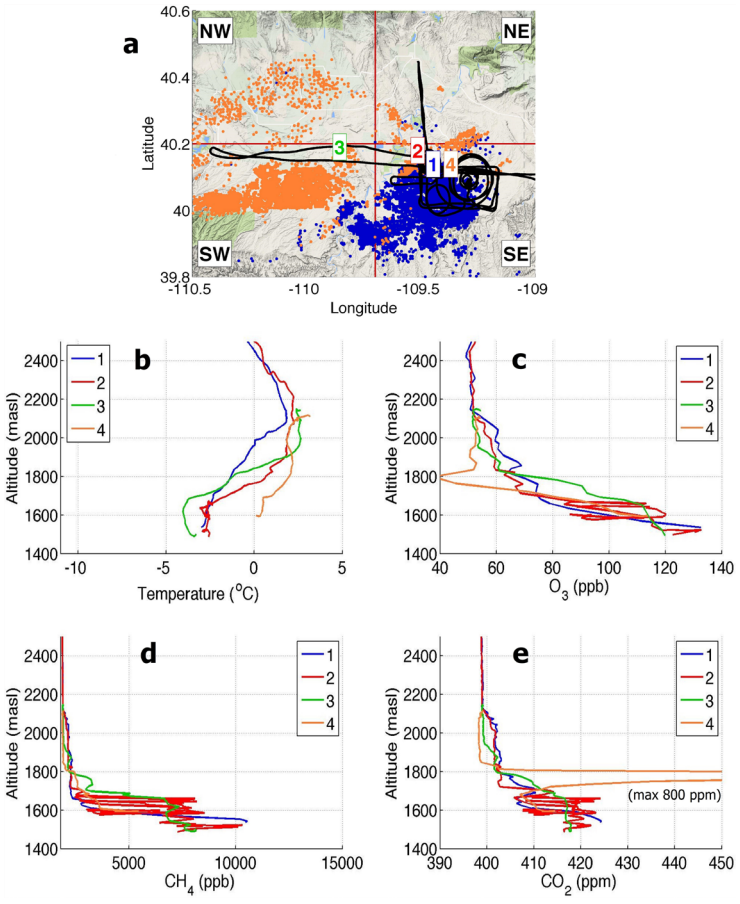

Figure 4

Vertical profile measurements in the Uinta Basin on 6 Feb. 2013.

Panel (a) Map of flight tracks and location of: (b) Temperature profiles, (c) O_3 profiles, (d) CH_4 profiles, (e) CO_2 profiles. Oil well locations are shown on the map as orange dots and gas wells as blue dots.

doi: 10.12952/journal.elementa.000132.f004

Measurements within the Bonanza power plant plume

On 6 February the flight track passed through the Bonanza power plant (located in the SE quadrant) plume and encountered enhanced CO_2 as observed in profile 4 in Figure 4e at an altitude of 1775–1850 m asl. CH_4 was not enhanced in the plume (Figure 4d) while O_3 was somewhat depleted (profile 4 in Figure 4c). The plume was located above the cold pool layer that topped out at ~170 m agl. Similar profile structure was seen on other flight days when the aircraft encountered the plume (Figure S2). Notably, the depression of O_3 mole fractions below values of O_3 measured outside the plume was most likely an indication of O_3 titration by NO emitted from the power plant as shown to be the case in other power plant plumes (Luria et al., 1999, 2003). The buoyant plume of emissions from the power plant, whose stack height is at 192 m agl above ground level or 1815 m asl, is lofted above the stack height (shown in a photograph on February 2 - Figure S3) but then descends somewhat as the plume cools and stabilizes above the top of the temperature inversion capped boundary layer. The combustion product CO_2 observed in the plume (and CO and NO_2 not shown) on each of these encounters declined abruptly immediately below the plume at the top of the cold pool layer, evidence that the plume was not adding substantially to O_3 precursor mole fractions in the cold pool layer and not likely to O_3 production below the inversion.

Spatial distribution of O_3, CH_4, NMHCs and other constituents

In 2012 O_3 mole fractions across the Basin varied over a relatively narrow range (~30–45 ppb) for the 13 flight days. CH_4, on the other hand showed a broader variation across the Basin (Figure S4). The location of the highest mole fractions varied from day to day (Figure S4), consistent with the variable wind conditions during the aircraft flights (Karion et al., 2013b). Peak CH_4 fell in the range 2500–3500 ppb.

In 2013 the buildup of O_3 mole fractions within the cold pool layer ≤1650 m asl across the entire expanse of the Basin during the episode of 31 January – 6 February is presented in Figure 5 and for CH_4 in Figure 6. Measurements above the top of the boundary layer inversion are not included in these plots. On 1 & 2 February (Figure 5b and c) the highest O_3 amounts were not coincident with the location of the main gas field (located in the south-east quadrant) while on 4, 5 and 6 February (Figure 5d, e and f) high O_3 (>120 ppb on 5 and 6 February) measured over the Basin included the gas field. A day

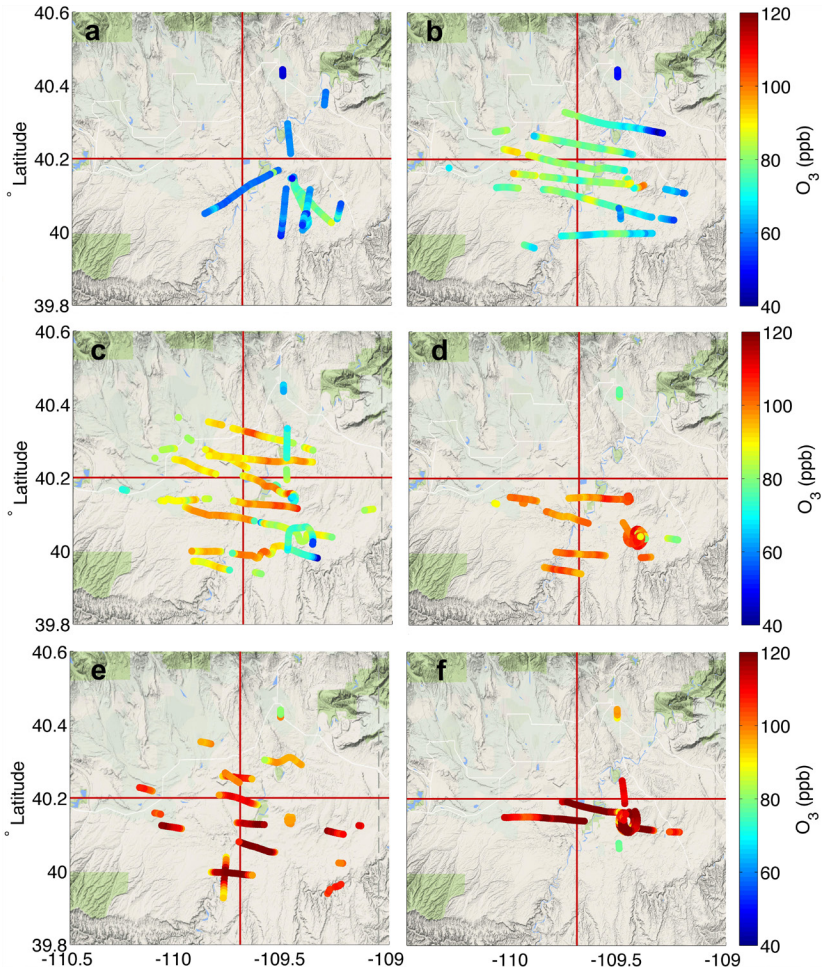

Figure 5

Map of flight tracks for O_3 in 2013 colored by mole fraction (ppb).

The flight tracks are for flight segments ≤1650 m asl. Panel (a) 31 Jan. (b) 1 Feb., (c) 2 Feb., (d) 4 Feb., (e) 5 Feb., (f) 6 Feb.

doi: 10.12952/journal.elementa.000132.f005

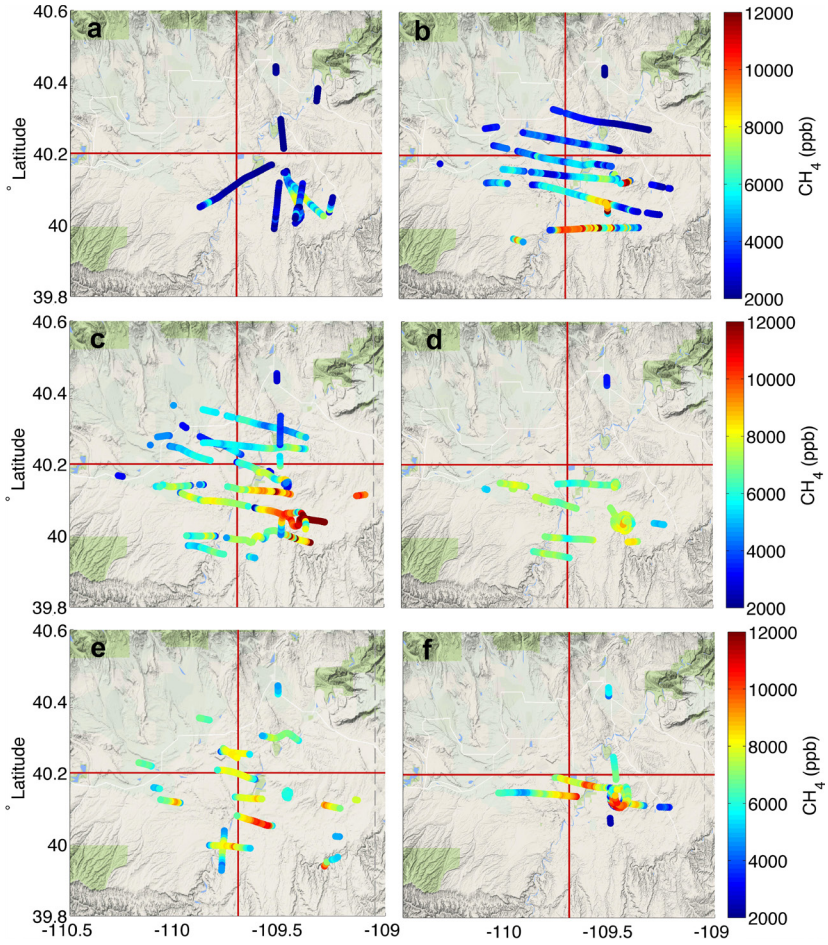

Figure 6

Map of flight tracks for CH_4 in 2013 colored by mole fraction (ppb).

The flight tracks are for flight segments ≤1650 m asl. Panel (a) 31 Jan. (b) 1 Feb., (c) 2 Feb., (d) 4 Feb., (e) 5 Feb., (f) 6 Feb.

doi: 10.12952/journal.elementa.000132.f006

to day increase across the entire Basin was observed. The spatial distribution of CH_4 was notably different from O_3 (Figure 6). On each day the highest mole fractions of CH_4 were found in the vicinity of the gas field spreading out over the rest of the Basin, indicative of a primary source location for the CH_4.

The mole fractions of O_3 precursor NMHCs in the Basin (measured from flasks collected on the aircraft) plotted against corresponding CH_4 mole fractions are presented in Figure 7. The data are plotted in colors by quadrant for 2013 and indicated by light grey circles for 2012. Note the lower concentrations of NMHCs in 2012 compared to 2013. Details on the correlations for 2013 are presented in Table 1. The regressions are two-sided accounting for errors in both variables.

Table 1. Correlation and slope of various non-methane hydrocarbons (NHMCs) and CO with methane determined from flask samples in 2013[a]

Compound	Slope (ppb/ppb)	Slope (mass fraction)	R^2	Slope (ppb/ppb) *Helmig et al., 2014*
ethane	0.066	0.124	0.98	0.063
propane	0.031	0.090	0.91	0.031
n-butane	0.011	0.029	0.89	0.0089
i-pentane	0.0045	0.016	0.93	0.0042
n-pentane	0.0041	0.015	0.84	0.0032
hexane	0.0027	0.012	0.84	0.0018
benzene	0.00070	0.0034	0.88	0.00058
heptane	0.0012	0.0075	0.76	
toluene	0.0010	0.0058	0.91	0.00064
octane	0.0006	0.0043	0.67	
m-,p-xylene	0.0003	0.0020	0.87	
CO	0.030		0.39	

[a]Regression is two-sided accounting for errors in both variables.

doi: 10.12952/journal.elementa.000132.t001

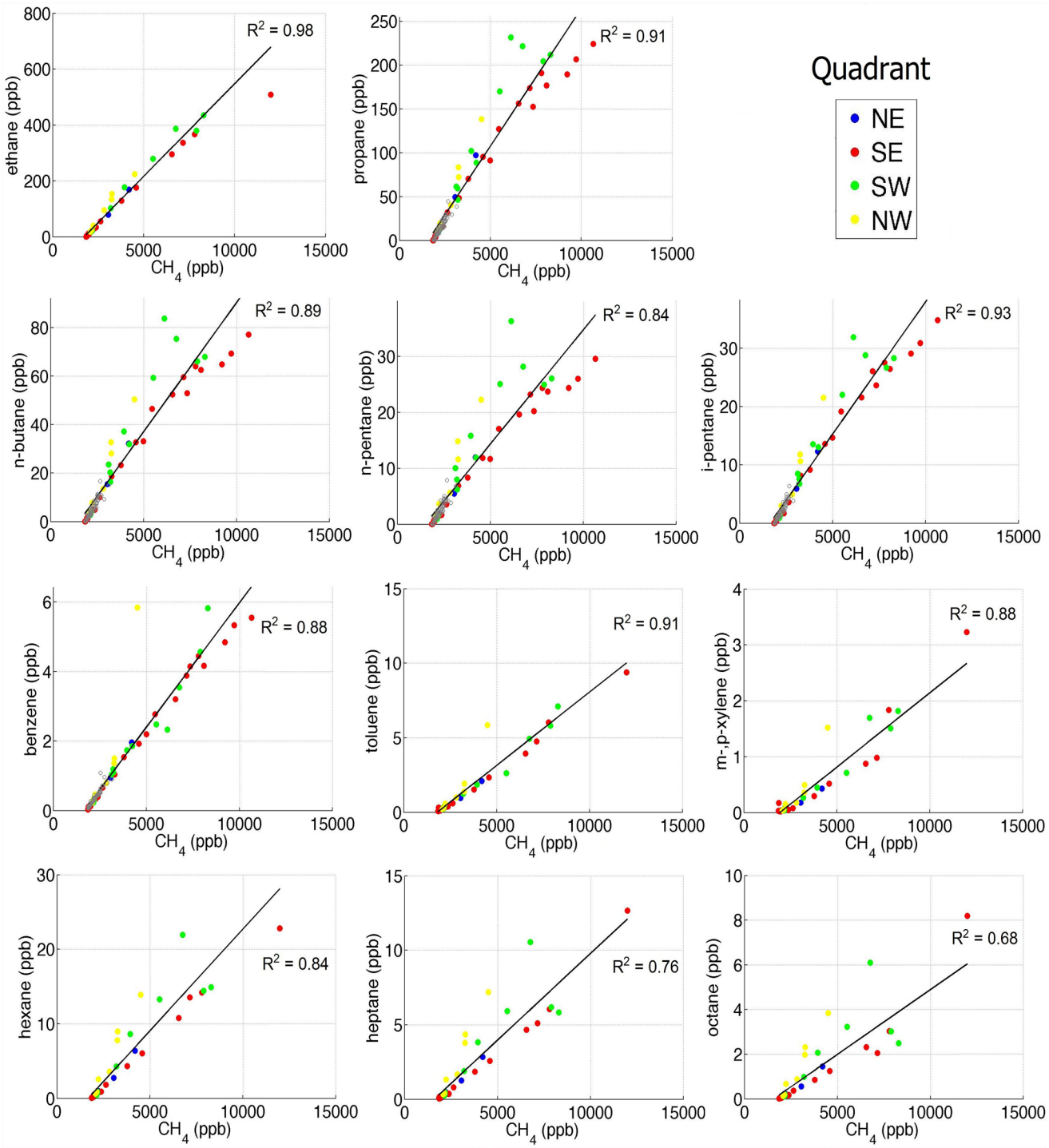

NMHCs and CH_4 (Figure 7 and Table 1) are tightly correlated, yielding linear regression R^2 results of 0.69 -.0.91. Although the NMHCs and CH_4 are similarly related in the two years, mole fractions are ~5 times greater in 2013 compared to 2012. Included in Table 1 are the mean NMHC/CH4 ratios that were observed at the Horsepool ground site in 2012 and 2013 (Helmig et al., 2014). There is a remarkably good agreement between these two data sets, with slope values generally agreeing to within ± 20%. The relatively close similarity in these results indicates that the surface observations from the Horsepool fixed ground site can be deemed relatively representative of the Basin. Another inference is that the NMHCs were distributed across the Basin in a similar manner to CH_4, and that they are co-emitted with CH_4 (Pétron et al., 2012; Peischl et al., 2013) when natural gas is vented or leaks into the atmosphere. The source of these emissions in the SE quadrant is consistent with the presence of a dense array of gas wells, gathering pipelines, compressor stations, and two large processing plants (Chipeta Plant Complex and Stagecoach/QEP) located in this quadrant. It is notable that for most of NMHC species, in particular the

Figure 7

Measurements of selected hydrocarbons plotted against CH_4 mole fraction.

Air samples collected in flasks over the Uinta Basin in 2013 (blue, red, green or yellow based on quadrant) and 2012 (light grey circles). The quadrants correspond to those shown in Figure 3a. Regression is two-sided accounting for errors in both variables. See Table 1 for slopes.

doi: 10.12952/journal.elementa.000132.f007

lighter NMHC, i.e. propane – pentane, show ~10–20% higher NMHC/CH_4 slope values for air originating in the SW quadrant compared to the SE. The in general lower NMHC/CH_4 values seen in the SE quadrant point towards a higher CH_4 fraction (dryer gas) in the fugitive emissions from that sector.

The average concentrations of O_3 and CH_4 within the cold pool beneath the temperature inversion for each day of aircraft measurements for the 2013 data presented in Figures 5 and 6 are plotted in Figure 8. On 31 January at the start of the event and just two days after the Basin had been swept out by the passage of a cold front, CH_4 mole fractions over the Basin were close to 3500 ppb This represents a significant enhancement above the mole fractions of ~1900 ppb measured above the boundary layer (Figure 3), which is similar to the regional background. By 2 February mean CH_4 mole fractions of 6800 ppb were spread throughout the Basin (Figure 6). Between 2 February and 5 February, average CH_4 mole fractions leveled off peaking at just over 7000 ppb, then decreasing to ~6000 ppb on 7 February. The leveling off and the subsequent decrease of CH_4 with the beginning of the Basin being flushed out is consistent with the time-behavior observed for CH_4 measurements at the surface made at Horse Pool (Edwards et al., 2014-extended data; Helmig et al., 2014).

Over the same time period, mean O_3 mole fractions increased (Figure 8) across the Basin. This was also seen in surface measurements (Helmig et al., 2014) and tether ozonesonde profiles (Schnell et al., 2016). On 31 January average O_3 mole fractions at 1650 m and below were ~60 ppb increasing steadily to ~110 ppb by 6 February before decreasing on 7 February with the approaching clean out event.

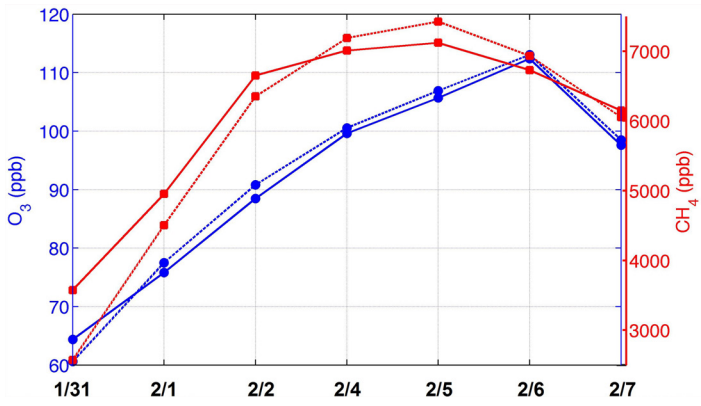

Figure 8

Concurrent CH_4 and O_3 for all observations ≤1650 m asl for seven flight days in winter 2013.

Mean (solid line) and median (dashed line) for each aircraft flight day of CH_4 (square symbol, red line) and O_3 (circle symbol, blue line). Observations were obtained from ~1100–1700 Mountain Standard Time.

doi: 10.12952/journal.elementa.000132.f008

Discussion

The multi-species aircraft profile measurements presented in this paper develop a picture of the relationship between various oil and gas field emissions within the Basin and their relationship to wintertime photochemical O_3 production. CH_4 and CO_2 were well correlated in the flight data both in 2012 (Figure S5) and 2013 (Figure 9) with the highest levels of both constituents measured in the vicinity of the gas field in the SE quadrant of the Basin. These correlations reflect a collocated source, with CH_4 directly emitted from extraction and gas processing while CO_2 is a product of combustion related activities also taking place in the vicinity of the gas field. High CO_2 values not corresponding to high CH_4 represent CO_2 sources without accompanying CH_4 such as power plant emissions or mobile sources (cars and trucks). This was seen most prominently in the NE quadrant in 2013 (Figure 9) where Vernal is located (the largest population center in the Basin with extensive vehicle traffic) and also in 2012 (Figure S5). Other constituents associated with combustion such as NO_2 and CO were not consistently related to CH_4 or each other in 2013 (Figure S6), likely due to additional chemical processing (NO_2) or other sources not related to CH_4 emissions (CO). In 2013 there is a strong tendency for higher O_3 mole fractions with higher CH_4 mole fractions throughout the Basin (Figure 10) reflecting the fact that O_3 precursor NMHCs are co-emitted with CH_4. However, there is a group of observations where O_3 was relatively constant with increasing CH_4. These observations are strongly concentrated in the SE quadrant. The highest mole fractions of NO_2 are also found in the SE quadrant (Figure S6). When the observations in Figure 10 are screened for NO_2 mole fractions greater than 10 ppb almost all of the observations where O_3 is relatively constant with increasing CH_4 drop out. This indicates the reduced efficiency of O_3 production in the presence of high NO_x mole fractions (Kleinman, 2005; Edwards et al., 2014; Ahmadov et al., 2015) and is consistent with the highest mole fractions of O_3 often being observed not in the immediate vicinity of the main gas field. O_3 mole fractions are moderately consistent with the variability in CO_2 (Figure 9) but do not show a consistent relationship with NO_2 or CO (Figure S7).

The contrasting meteorological conditions during the winters of 2012 and 2013 highlight the way these conditions led to only modest O_3 formation in winter 2012 and to the extreme high O_3 episodes

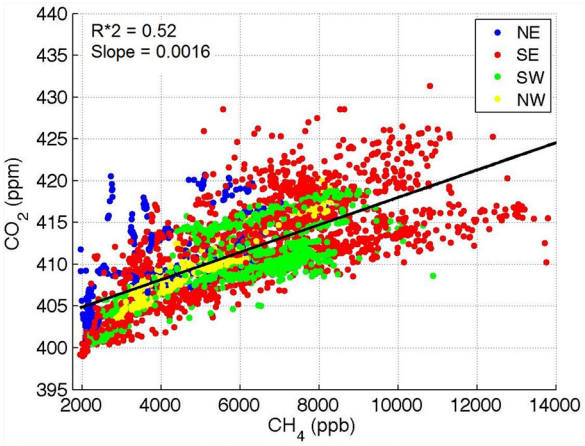

Figure 9

CO_2 mole fraction as a function of CH_4 mole fraction in winter 2013.

Aircraft measurements ≤1650 m asl color coded based on the quadrant where the measurement was made. Values are 5 second averages. The quadrants are those shown in Figure 3a. Regression is two-sided accounting for errors in both variables.

doi: 10.12952/journal.elementa.000132.f009

in winter 2013. The contrasting temperature and constituent profiles between 2012 (Figure 3) and 2013 (Figure 4) show that the air confining geographic characteristics of the Basin also require conditions that prevent efficient vertical mixing and ventilation of air out of the Basin as occurred in 2012. It is worth noting that in 2012 when there was little snow on the ground almost all the incoming radiant heating was transferred to an outgoing heat flux with very little loss to latent heating (R. Zamora, private communication; Stoeckenius and McNally, 2014). Although the ground was snow-covered in 2013 (Oltmans et al., 2014) and daytime temperatures were always relatively cold, a cold pool up to ~200 m thick with nearly constant temperature and constituent mole fractions indicated a mixed layer resulting from daytime heating of the surface and convective mixing. It was within this layer that the highest mole fractions of constituents emitted from the surface as well as elevated O_3 were measured.

In air above this mixed layer, mole fractions of all constituents declined to values representative of background levels. Assuming that CH_4 emissions remain relatively constant in the Basin and due to the long chemical lifetime of CH_4, the stabilization of CH_4 mole fractions after the first few days of the episode (Figure 8) is consistent with some advection of air out of the Basin. However, O_3 mole fractions continued to increase (Figure 8) across the Basin through the flight period (also seen in other surface and profile measurements; Helmig et al., 2014; Schnell et al., 2016). During the course of the O_3 event, nighttime O_3 minimum values continued to rise (Figure 2 and Schnell et al., 2016), indicating that nighttime chemical loss, surface deposition, and transport out of the boundary layer did not fully remove O_3 from the previous day's production. Although CH_4 (and likely also accompanying NMHC) levels stabilized after a few days, they remained sufficiently high to fuel O_3 production and increasing O_3 mole fractions throughout the event captured by the aircraft flights.

The spatial pattern of emitted constituents in 2013, such as CH_4 (Figure 6) and CO_2 (Figure S8), is indicative of strong emissions in the region of the natural gas field in the SE quadrant of the Basin that spread throughout the Basin. Wind measurements throughout the Basin are supportive of this (Schnell et al., 2016) where a diurnal wind pattern in which daytime heating at the edge of the Basin moves air from the central portion of the Basin toward the periphery. Based on the CH_4 and aircraft flask-sampled NMHCs, this transport pattern dispersed precursors throughout the Basin. The availability of O_3 precursors throughout the Basin was reflected in the high O_3 mole fractions that encompass the entire Basin

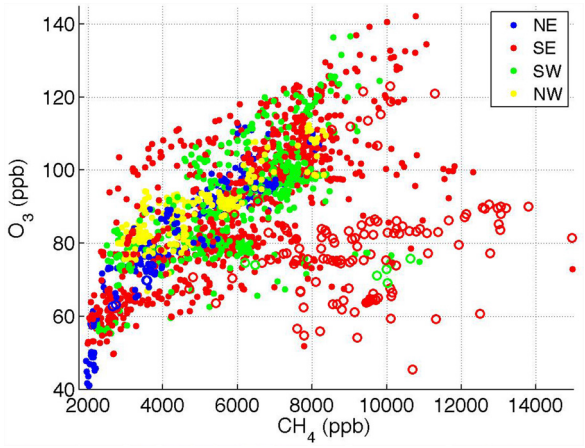

Figure 10

O_3 mole fraction as a function of CH_4 mole fraction in winter 2013.

All aircraft measurements for altitudes ≤1650 m asl. The measurements are color coded based on the quadrant where the measurement was made. The quadrants are those shown in Figure 3a. Values are 5 second averages. Observations with NO_2 > 10 ppb are designated by open circles.

doi: 10.12952/journal.elementa.000132.f010

and were not concentrated around the primary source of the precursors (Figure 5) where very high NO_x levels may influence the O_3 production efficiency. On several days the highest O_3 mole fractions were encountered away from the gas field, consistent with the time scales for O_3 production that are not instantaneous. This O_3 spatial pattern in the Basin was a result of strong photochemical production over the entire Basin, not primarily a result of transport from a more localized source near where the precursors were emitted.

The tight relationship between CH_4 and NMHCs in both ground and aircraft data (Table 1) and the magnitude of the reported methane (Karion et al., 2013b) and NMHC (Helmig et al., 2014) emissions suggests that the eventual dispersal of the basin wide natural gas related emissions contribute to the atmospheric methane and NMHC increases that have recently been reported on a broader geographical scale (Helmig et al., 2016; Turner et al., 2016).

Summary

Extensive aircraft sampling of O_3, CH_4, CO, and NO_2, along with numerous gas species from flask measurements, during the winters of 2012 and 2013, demonstrated the strongly contrasting conditions in both the spatial and vertical dimensions of wintertime O_3 production in these two years. In 2012 O_3 mole fractions were confined to a narrow range of 30–45 ppb throughout the Basin with only small variations with altitude to the top of the measured profiles that extended to above the rim of the Basin. In 2012 CH_4 across the Basin varied from flight-to-flight, although the highest levels were found near the gas field and in a pattern where CH_4 was higher in the direction of the prevailing winds (Karion et al., 2013b). O_3, on the other hand, was much more uniform over the Basin reflecting the lack of connection with precursor emissions under conditions with minimal O_3 production.

The strongest O_3 production in 2013 occurred in a shallow surface layer with a strong temperature inversion topped near 1650±50 m asl. Above the cold pool was a gradient layer extending to ~2200 m asl with elevated constituent mole fractions that gradually declined to near lower free tropospheric values.

The structure of constituent profiles measured through the plume of a power plant located in the eastern portion of the Basin did not identify a pathway for mixing chemical precursors found in the power plant plume, which was emitted far above the O_3 maximum, into the boundary layer. Also, since the enhancements in O_3 and emitted constituents were always seen in the layer below the top of the temperature inversion, there is strong evidence that the source of these enhancements was from within the Basin itself.

The contrast seen in the aircraft measurements between 2012 and 2013 demonstrates the dominant role snow cover plays in promoting winter O_3 production in the Uinta Basin. Modeling of the conditions in the 2011–2012 and 2012–2013 winters (Edwards et al., 2013; Neemann et al., 2015; Edwards et al., 2014; Ahmadov et al., 2015) supports the vital role snow cover has on wintertime ozone production as this promotes and sustains strong temperature inversions that leads to highly elevated mole fractions of ozone precursors (Schnell et al., 2009). The snow also enhances UV flux because of its high surface albedo and snow reduces O_3 deposition to the surface. Based on precursor emission levels and meteorological conditions in 2013 and similar conditions observed in 2010 and 2011 in the Uinta Basin (Oltmans et al., 2014), it is likely that high O_3 episodes can be expected in the future under snow-covered conditions if emissions from oil and gas operations remain at 2013 levels in the Uinta Basin in future winters.

References

Ahmadov R, McKeen S, Trainer M, Banta R, Brewer A, et al. 2015. Understanding high wintertime ozone in oil and natural gas producing region of the western U.S. *Atmos Chem Phys* **15**: 411–429. doi: 10.5194/acp-15-411-2015.

Bader DC, McKee TB. 1985. Effects of shear, stability and valley characteristics on the destruction of temperature inversions. *J Clim Appl Meteorol* **24**: 822–832.

Chameides WL, Fehsenfeld F, Rodgers MO, Cardelino C, Martinez J, et al. 1992. Ozone precursor relationships in the ambient atmosphere. *J Geophys Res-Atmos* **97**(D5): 6037–6055.

Edwards PM, Young CJ, Aikin K, deGouw J, Dubé WP, et al. 2013. Ozone photochemistry in and oil and natural gas extraction region during winter: Simulations of a snow-free season in the Uintah Basin, Utah. *Atmos Chem Phys* **13**: 8955–8971. doi: 10.5194/acp-13-8955-2013.

Edwards PM, Brown SS, Roberts JM, Ahmadov R, Banta RM, et al. 2014. High winter ozone pollution from carbonyl photolysis in an oil and gas Basin. *Nature* **514**: 351–354. doi: 10.1038/nature13767.

Gilman JB, Lerner BM, Kuster WC, de Gouw JA. 2013. Source signature of volatile organic compounds from oil and natural gas operations in Northeastern Colorado. *Environ Sci Tech* **47**: 1297–1305. doi: 10.1021/es304119a/.

Helmig D, Bottenheim J, Galbally IE, Lewis A, Milton MJT, et al. 2009. Volatile organic compounds in the global atmosphere. *EOS Transactions of the American Geophysical Union* **90**: 513–514. doi: 10.1029/2009EO520001.

Helmig D, Rossabi D, Hueber J, Tans P, Montzka SA, et al. 2016. Reversal of global atmospheric ethane and propane trends largely due to US oil and natural gas production, *Nature Geosci* **9**: 490–495. doi: 10.1038/ngeo2721.

Helmig D, Thompson C, Hueber J, Park J-H. 2014. Highly elevated levels of volatile organic compounds in the Uintah Basin, Utah. *Environ Sci Technol* **48**: 4707–4715. doi: 10.1021/es405046r.

Karion A, Sweeney C, Wolter S, Newberger T, Chen H, et al. 2013a. Long-term greenhouse gas measurements from aircraft. *Atmos Meas Tech* **6**: 511–526.

Karion A, Sweeney C, Petron G, Frost G, Hardesty RM, et al. 2013b. Methane emissions estimate from airborne measurements over a western United States natural gas field. *Geophys Res Lett* **40**: 4393–4397. doi: 10.1002/grl.50811.

Kleinman LI. 2005. The dependence of tropospheric ozone production rate on ozone precursors. *Atmos Environ* **39**: 575–586.

Lareau NP, Crosman E, Whiteman CD, Horel JD, Hoch SW, et al. 2012. The persistent cold-air pool study. *Bull Am Meteor Soc* **94**: 51–63. doi: 10.1175/BAMS-D-11-00255.1.

Luria M, Imhoff RE, Valente RJ, Tanner RL. 2003. Ozone yields and production efficiencies in a large power plant plume. *Atmos Environ* **37**: 3593–3603. doi: 10.1016/s1352-2310(03)00342.

Luria M, Valente RJ, Tanner RL, Gillani NV, Imhoff RE, et al. 1999. The evolution of photochemical smog in a power plant plume. *Atmos Environ* **33**(18): 3023–3036. doi: 10.1016/S1352-2310(99)00072-2.

Lyman S, Shorthill H, eds. 2013. Final Report: 2012 Uintah Basin Winter Ozone & Air Quality Study. *Doc. No. CRD13-320.32, Commercialization and Regional Development, Utah State University, 1 February*. http://rd.usu.edu/files/uploads/ubos_2011-12_final_report.pdf.

Neemann EM, Crosman ET, Horel JD, Aver L. 2015. Simulations of a cold-air pool associated with elevated wintertime ozone in the Uintah Basin, Utah. *Atmos Chem Phys* **15**: 135–151. doi: 10.5194/acp-15-135-2015.

NOAA GMD Aircraft. http://www.esrl.noaa.gov/gmd/ccgg/aircraft/analysis.html.

Oltmans S, Schnell R, Johnson B, Pétron G, Mefford T, et al. 2014. Anatomy of wintertime ozone production associated with oil and gas extraction activity in Wyoming and Utah. *Elem Sci Anth* **2**: 000024. doi: 10.12952/journal.elementa.000024.

Ollison WM, Crow W, Spicer CW. 2014. Field testing of new-technology ambient air monitors. *Journal of the Air and Waste Management Association* **63**: 855–863.

Peischl J, Ryerson TB, Holloway JS, Trainer M, Andrews A, et al. 2013. Quantifying sources of methane using light alkanes in the Los Angeles Basin, California. *J Geophys Res-Atmos* **118**: 4974–4990. doi: 10.1002/grd50413.

Pétron G, Frost G, Miller BR, Hirsch AI, Montzka SA, et al. 2012. Hydrocarbon emissions characterization in the Colorado Front Range: A pilot study. *J Geophys Res* **117**(D4). doi: 10.1029/2011JD016360.

Rappenglück B, Ackermann L, Alvarez S, Golovko J, Buhr M, et al. 2014. Strong wintertime ozone events in the Upper Green River, Wyoming. *Atmos Chem Phys* **14**: 4909–4934. doi: 10.5194/acp-14-4909-2014.

Schnell RC, Oltmans SJ, Neely RR, Endres MS, Molenar JV, et al. 2009. Rapid photochemical production of ozone at high concentrations in a rural site during winter. *Nature Geosci* **2**: 120–122. doi: 10.1038/ngeo415.

Schnell RC, Johnson BJ, Oltmans SJ, Cullis P, Sterling C, et al. 2016. Quantifying ozone production throughout the boundary layer from high frequency tethered profile measurements during a high ozone episode in the Uinta Basin, Utah. *J Geophys Res Atmos*. doi: 10.1002/2016JD025130.

Stoeckenius T, McNally D, eds. 2014. Final Report 2013 Unita Basin Winter Ozone Study. http://www.deq.utah.gov/locations/uintahBasin/studies/UBOS-2013.htm.

Turner AJ. Jacob DJ, Benmergui J, Wofsy SC, et al. 2016, A large increase in U.S. methane emssions over the past decade inferred from satellite data and surface observations. *Geophys, Res. Lett* **43**: 2218-2224. doi: 10.1002/2016GL067987

Utah Oil and Gas Program. http://oilgas.ogm.utah.gov/.

Warneke C, Geiger F, Edwards PM, Dube W, Pétron G, et al. 2014. Volatile organic compound emissions from the oil and natural gas industry in the Uinta Basin, Utah: Point sources compared to ambient air composition. *Atmos Chem Phys* **14**: 10977–10988. doi: 10.5194/acp-14-10977-2014.

Yu C-H, Pielke RA. 1986. Mesoscale air quality under stagnant synoptic cold season conditions in the Lake Powell area. *Atmos Environ* **20**: 1751–1762.

Contributions

- Contributed to conception and design: CS, RCS, AK
- Contributed to acquisition of data: CS, AK, SW, DN, SAM, BRM, DH, BJJ, JH, SC
- Contributed to analysis and interpretation of data: SJO, AK, RCS, GP, CS, DH, SAM
- Drafted and/or revised the article: SJO, AK, RCS, CS, GP, DH, SAM
- Approved the submitted version of the article: SJO, AK, RCS, CS, GP, DH, SW, DN, SAM, BRM, BJJ, JH, SC

Acknowledgments

The NO_2 analyzer used on the aircraft was generously loaned to NOAA/GMD by Russ Dickerson of the University of Maryland. The skilled piloting of the aircraft by Chuck Midyett and Steve Conley was a key element in obtaining the extensive data set used in this study.

Funding information

Funding for the aircraft flights was provided by the NOAA Climate Program Office. Partial funding for the purchase of the NO_2 analyzer was provided through Russ Dickerson's participation in the NASA AQAST program. The 2013 Uintah Basin Ozone Study was funded by and provided in-kind support by the: Uintah Impact Mitigation Special Service District (UIMSSD), Western Energy Alliance, QEP Resources, Inc., Bureau of Land Management (BLM), National Oceanic and Atmospheric Administration (NOAA), Environmental Protection Agency (EPA), Utah Department of Environmental Quality (UDEQ) and Utah Science Technology and Research Initiative (USTAR), and Utah School and Institutional Trust Lands Administration (SITLA).

Competing interests

The authors do not have any competing interests that might influence the interpretation of the manuscript.

Data accessibility statement

Data sources are cited in the text of the manuscript with the URLs listed in the references.

Supplemental figures

- **Figure S1. Photograph of the Cessna 210 aircraft.**
  The aircraft sampled over the Uinta Basin in February 2013. Three inlets and two temperature and humidity probes were installed under the starboard wing. Photo credit: Colm Sweeney, CIRES, NOAA GMD.
- **Figure S2. Profile measurements in the Uinta Basin on Panel (A) 31 Jan., (B) 1 Feb., (C) 2 Feb., (D) 4 Feb. 2013.**
  Panel (a) Map of flight tracks and location of: (b) Temperature profiles. (c) O_3 profiles, (d) CH_4 profiles, (e) CO_2 profiles.
- **Figure S3. Photograph taken from the aircraft of the Bonanza Power Plant on 2 February 2013.**
  The plume rises above the inversion layer defined by the haze below the inversion. Photo credit: Colm Sweeney, CIRES, NOAA GMD.
- **Figure S4. Flight tracks for CH_4 in 2012 colored with mole fractions in ppb.**
  The flight tracks are for all altitudes below 2500 m asl. The flight date is indicated above each panel (YYYYMMDD).
- **Figure S5. CH_4 mole fractions as a function of CO_2 mole fractions on 9 February 2012.**
  The data are color coded by vertical profile segment. All flight altitudes are included. The grey dots are for portions of the flight not included in the profile segments. High CO_2 values not corresponding to high CH_4 represent CO_2 sources without accompanying CH_4 such as power plant emissions or mobile sources (cars and trucks).
- **Figure S6. CH_4 versus NO_2, CH4 versus CO, and NO_2 versus CO for all flight days in 2013 color coded by quadrant.**
  The data are for portions ≤1650 m asl.
- **Figure S7. Relationship between CO_2 and O_3, NO_2 and O_3, and CO and O_3 over the different quadrants of the Basin in 2013.**
  Data are for altitudes ≤ 1650 m asl.
- **Figure S8. Map of flight tracks for CO_2 in 2013 colored by mole fraction (ppb).**
  The flight tracks are for portions ≤1650 m asl. Panel (a) 31 Jan. (b) 1 Feb., (c) 2 Feb., (d) 4 Feb., (e) 5 Feb., (f) 6 Feb.